Modeling the impact of defects on the charge collection efficiency of a Cadmium Telluride detector

Golovleva, M.

2021-08-01

Golovleva , M , Bezak , M , Bharthuar , S , Brücken , E , Gädda , A , Härkönen , J , Kalliokoski , M , Kirschenmann , S , Luukka , P , Ott , J & Tuuva , T 2021 , ' Modeling the impact of defects on the charge collection efficiency of a Cadmium Telluride detector ' , Journal of Instrumentation , vol. 16 , no. 8 , P08027 . https://doi.org/10.1088/1748-0221/16/08/p08027

http://hdl.handle.net/10138/346540
https://doi.org/10.1088/1748-0221/16/08/p08027

acceptedVersion

PREPARED FOR SUBMISSION TO JINST

Modeling the impact of defects on the charge collection efficiency of a Cadmium Telluride detector

---

M. Golovleva,[a,b,1] **M. Bezak**[a,b] **S. Bharthuar**[a] **E. Brücken**[a] **A. Gädda**[a,c] **J. Härkönen**[a,e]
M. Kalliokoski[a,f] **S. Kirschenmann**[a] **P. Luukka**[a,b] **J. Ott**[a,d] **T. Tuuva**[b]

[a] *Helsinki Institute of Physics,*
Gustaf Hällströmin katu 2, FI-00014 University of Helsinki, Finland
[b] *Lappeenranta University of Technology,*
Skinnarilankatu 34, FI-53850 Lappeenranta, Finland
[c] *Okmetic Oy,*
Piitie 2, FI-01510 Vantaa Finland
[d] *Aalto University, Department of Electronics and Nanoengineering,*
Tietotie 3, FI-02150 Espoo, Finland
[e] *Ludong University,*
186 Hongqi W Rd, Zhifu District, Yantai, Shandong, China
[f] *Ruđer Bošković Institute, Bijenička cesta 54, HR-10000 Zagreb, Croatia*

E-mail: maria.golovleva@lut.fi

ABSTRACT: Cadmium telluride is a favorable material for X-ray detection as it has an outstanding characteristic for room temperature operation. It is a high-Z material with excellent photon radiation absorption properties. However, CdTe single crystals may include a large number of extended crystallographic defects, such as grain boundaries, twins, and tellurium (Te) inclusions, which can have an impact on detector performance. A Technology Computer Aided Design (TCAD) local defect model has been developed to investigate the effects of local defects on charge collection efficiency (CCE). We studied a 1 mm thick Schottky-type CdTe radiation detector with transient-current technique by using a red laser at room temperature. By raster scanning the detector surface we were able to study signal shaping within the bulk, and to locate surface defects by observing their impact on the CCE. In this paper we present our TCAD model with localized defect, and compare the simulation results to TCT measurements. In the model an inclusion with a diameter of 10 μm was assumed. The center of the defect was positioned at 6 μm distance from the surface. We show that the defect has a notable effect on current transients, which in turn affect the CCE of the CdTe detector. The simulated charge collection at the position of the defect decreases by 80 % in comparison to the defect-free case. The simulations show that the defects give a characteristic shape to TCT signal. This can further be used to detect defects in CdTe detectors and to estimate the overall defect density in the material.

KEYWORDS: X-ray detectors, Detection of defects, Simulation methods and programs

---

[1] Corresponding author.

Contents

1 Introduction 1

2 Materials and Methods 2
2.1 TCAD simulations 2
2.2 TCT measurements 3

3 Results and discussion 4
3.1 Simulation results 4
3.2 Experimental results 9

4 Conclusions 11

1 Introduction

Cadmium Telluride (CdTe) is a suitable material for room temperature detection of X-ray and gamma-ray radiation. It has a relatively large band gap, 1.47 eV at 300 K, resulting in a small thermal noise. Another outstanding characteristic of this semiconductor material is its high atomic number that enables strong absorption and good detection efficiency for high-energy photons [1, 2].

At the same time, CdTe detectors suffer from the crystal impurities such as Te-inclusions, dislocation networks, and twin and subgrain boundaries [3], which affect the detector performance [4, 5]. Defects and impurities at the grain boundaries can trap charge carriers and also act as charge drains, which can be seen as fluctuations in the collected signal and charge collection efficiency (CCE) [6].

Laser Transient Current Technique (TCT) is a widely used and adopted method for the characterisation of semiconductor radiation detectors. TCT reveals many material characteristics of a detector, including defects and their influence on electric properties of the device [7, 8].

During a TCT measurement, a laser pulse generates charge carriers which pass through the detector in the applied electric field. With red laser TCT, electron-hole pairs (*e*-*h* pairs) are generated close to the surface of the illuminated side of the device. One type of the charge carriers is immediately collected by the nearest electrode. Thus, the induced current is an outcome of a single carrier type drift, depending on the bias voltage. The collected signal is rich on information about the detector: various parameters, such as rise time, charge collection efficiency (CCE), and peaking amplitude can be extracted from the signal. By mounting the setup on a XYZ-stage and by combining the signal output with the position information from the stage, the locations of the defects and other non-uniformities can be mapped, and their effect on the charge collection efficiency (CCE) can be studied [9].

In this paper, we studied the effects of defects in CdTe pad detectors by using red laser TCT. In order to identify the impact of defects on the transient currents, simulations of a CdTe diode structure with the defect inclusion has been performed. By combining measured results and TCAD simulations a detailed study of detector performance was obtained.

2 Materials and Methods

2.1 TCAD simulations

To better understand the impact of the defects on the detector performance, simulations were made using a Technology Computer Aided Design (TCAD) package from Synopsys [10]. The TCAD package provides the ability to simulate 2D or 3D CdTe structures with various electrode geometries and uses a drift diffusion model to simulate the detector response. At each point of the model, the Poisson and the charge carrier continuity equations are solved and the electrostatic potential and the carrier concentrations are calculated.

The simulated diode structure had dimensions of A x 3000 x 1000 μm^3 with a 50 nm thick AlN passivation layer, where A is an area factor to match the dimensions of the real diode. The thicknesses of the gold contacts on the front and backplanes were 500 nm. A work function of 5 eV for Schottky-type contacts was assumed. In the simulation, CdTe bulk with a uniform charge carrier concentration of 1×10^7 cm^{-3} was used [11]. A bias voltage of -450 V from the backplane was utilised in the simulations and the front plane was set to ground. To consider the high defect concentrations in the CdTe bulk, two mid-gap levels (a deep acceptor and a donor level) were implemented with energies of 0.72 eV and with a concentration of 1×10^{12} cm^{-3} [12]. The electron and hole capture cross sections were found by fitting simulated transients to the measurement results.

As revealed by IR microscopy mid-sized Te inclusions are in 5 - 15 μm range [13, 14]. In the simulations, large-scale defects (grain boundaries, Te inclusions) in the detector bulk were reproduced by introducing a CdTe semiconductor material inclusion with high amount of traps into the detector body, as depicted in Fig. 1b. This approach was used since the conventional method of introducing energy levels into the CdTe bulk bandgap does not provide any physical localization of the defects. Due to this, a circular shaped inclusion with a diameter of 10 μm was considered as a local defect imitation. For the trap levels in the inclusion material, the same two mid-gap levels (a deep acceptor and a donor level) were implemented with energies of 0.72 eV.

The laser excitation was applied to the front opening. For the generation-recombination mechanism of charge carriers in the CdTe, the doping-dependent Shockley-Read-Hall model (Scharfetter relation [10]) and impact ionization (van Overstraeten model [16]) were used in the simulation. The penetration depth of a red laser is about a few μm, so the red laser TCT signal displays holes drifting through the device, while electrons are immediately collected away by the front contact. The red laser current pulses can be described by the Ramo–Shockley theorem [17]:

$$I_{e,h}(t) = N_{e,h} \exp \frac{-t}{\tau_{e,h}} \vec{E}(\vec{r}) \vec{E}_w(\vec{r}), \tag{2.1}$$

where $N_{e,h}$ is effective doping concentration, $\vec{r}$ the location of the charge, $\tau_{e,h}$ is effective carrier trapping time, $\vec{E}(\vec{r})$, the weighting field given by the electrode configuration in the detector [9]. To consider electric field variation near the surface, the laser beam was pointed at 3 different positions at the surface: the middle of the optical opening (0), the left and right edge of the opening (550 and -550).

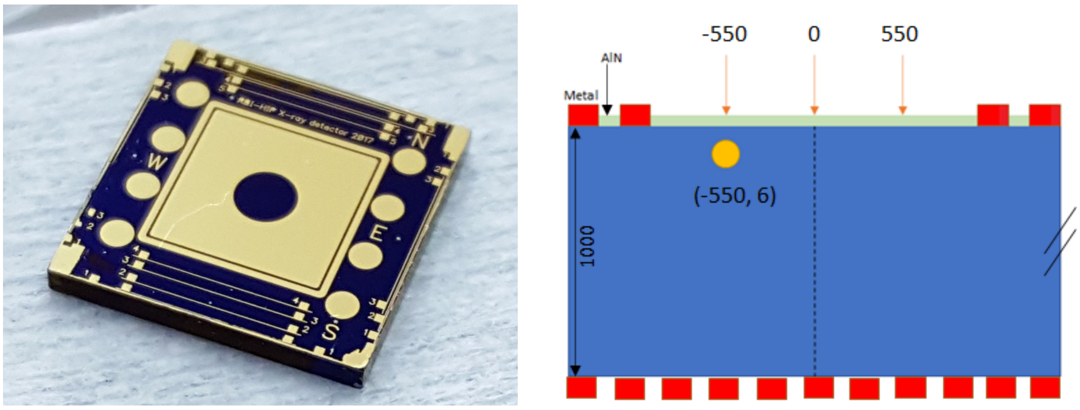

(a) (b)

Figure 1: a) A pad detector with an optical opening in the middle [15] and b) a schematic of the simulated structure with the optical opening and a defect inclusion. All the dimensions are in μm. Optical opening is from -1000 μm to 1000 μm and the defect inclusion center position is (-550, 6). The laser beam was pointed at 3 different positions at the surface: the middle of the opening (0), the left and right edge of the opening (-550 and 550).

2.2 TCT measurements

The CdTe pad detectors discussed in this paper represent a simple structure of a CdTe single crystal with metal electrodes on both sides. Prior to metallization, CdTe was passivated with aluminium nitride (AlN) [15, 18]. The contacts for both sides of CdTe detector were formed by sputtering depositions resulting in Schottky barrier contacts. They consist of a 20 nm thick titanium tungsten (TiW) adhesion layer, and around 200 nm thick layer of gold. For TCT measurements, there is an optical opening on the front side with a diameter of 2 mm without any metallization (Fig. 1a).

The TCT-setup consists of a pulsed laser source, optics with an adjustable diaphragm collimator, and a XYZ-stage. The detectors were mounted to the XY-plane of the system by pressing the front anode with a wire. The wire was also used as a contact for the detector bias. The backside of the detectors was grounded through the metal frame of the sample holder.

The bias voltage of +450 V was provided with a Keithley 2410 SourceMeter through a bias-T to the front contact. The voltage supply was also used to monitor, and to limit, the leakage current of the system. The output signal was passed through the bias-T to a Particulars AM-01 A 53 dB RF-amplifier. The resulting signal pulses were read out with a Teledyne Lecroy WaveRunner 840M-MS, 4 GHz, oscilloscope. The oscilloscope was operated in a sampling mode with a sampling frequency of 20 GS/s and a running average of 50 measurements, which was selected experimentally as a balance between noise suppression and response to changes in rise time. All measurements were made at room temperature.

A pulsed red-laser (wave length 660 nm, power 10 mW) with a Gaussian beam profile and pulse duration of 440 ps was used for *e*-*h* pair creation. The repetition rate was set to 50 Hz and pulse power was cut to 60% of the maximum power, yielding pulse energy of about 4.4 pJ. The focal distance of the laser was set with a knife-edge technique [19].

In order to locate areas with non-uniformities, the optical opening of the detectors was raster scanned. From the TCT signals, values of amplitude, charge collection efficiency, peaking time, and rise time, were extracted and mapped in 2D maps using the coordinate information from the stages. From the maps, areas with defects were identified [20]. The CCE is defined as an integral over the transient current signal with a time window of 900 ns. The resulting values are then normalized to the highest value in the measured area.

3 Results and discussion

3.1 Simulation results

In order to investigate the impact of the defect inclusion on the electrical field and the transient currents, a simulation of a reference diode detector with no bulk defects, no surface passivation layer on top of the optical opening and no incorporated defect inclusion was performed. This model is compared to the same structure with one defect inclusion inside.

In Fig. 2, the transverse distribution of the electrical field at the position of the defect is depicted for the abovementioned structure. The local defect introduction of a circular shape at the position of (-550, 6) gives us a fluctuation of the electric field due to charge accumulation as consequence of carrier trapping by the trap levels in the inclusion. In Fig. 2a one can see that the electric field starts increasing from the value of 1.7 kV/cm near the surface, while for the case without any defect, inclusion the value for the electric field near the surface is 2.1 kV/cm. Figure 2b shows that there is a disturbance of the electrical field at the position of the defect inclusion in the lateral distribution as well. This initial simulation indicates that the presence of a localised defect inclusion near the surface can cause fluctuations of the electric field, resulting in a change of the outcome signal.

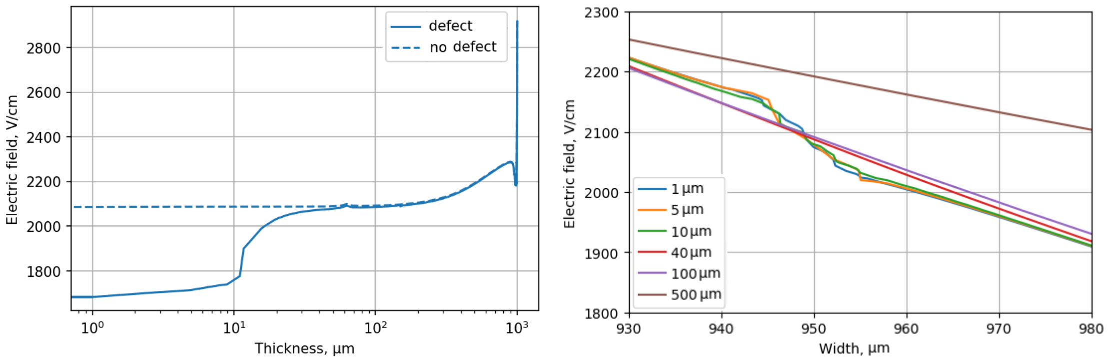

(a)

(b)

Figure 2: a) Comparison of the simulated transverse distribution of the electrical field at the position of the defect for the simulated diode with and without defect incorporation. No bulk traps and no surface passivation were considered. b) Simulated lateral electric field cuts with defect incorporated for different distances from the surface in μm in the proximity of the defect position.

The transient currents of the CdTe diode with and without defect are shown in Fig. 3. In the case of no inclusion, after generating $e - h$ pairs, fast electrons are collected on the front electrode in a short time that is demonstrated as a narrow peak, whereas slow holes travel long time through the sample to the back. When we are looking at the transient with the local defect, after the narrow peak produced by collected electrons the current rapidly decreases. In Fig. 3b the zoomed plot of the transient current is depicted. As the creation point of $e-h$ pairs is very close to the defect area with a very high concentration of traps, part of the free carries were captured by the trap levels in the inclusion. As it is shown in Fig. 3, the current for the case with the defect is by 2 orders of magnitude less than the signal without any inclusion.

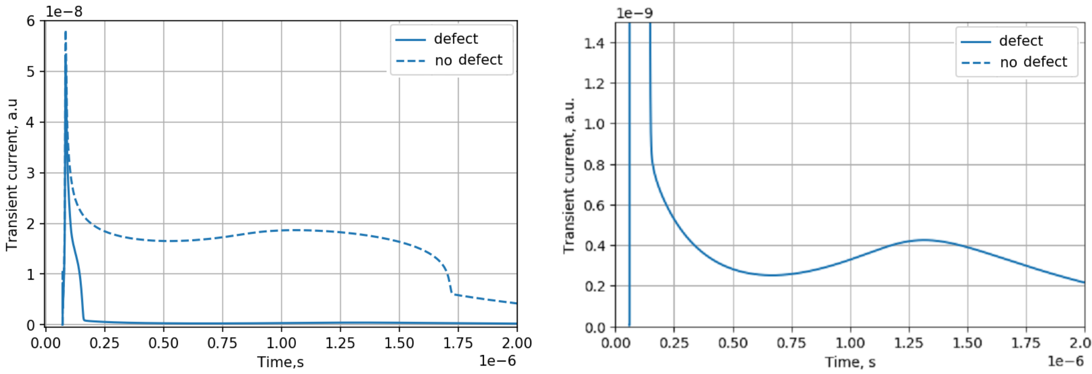

(a) (b)

Figure 3: a) Comparison of the simulated transient current at the position of the defect for simulated diode with and without defect incorporation. No bulk traps and no surface passivation were considered. b) Zoom-in to the transient with defect inclusion.

In addition to bulk defects, surface recombination has a high impact on the device performance [21]. This can be reduced by passivating the surfaces of the crystal. To see how it affects the field strength, the AlN layer is added on top of the optical opening of the simulated structure. In Fig. 4a, the transverse distribution of the electrical field is compared for two cases: passivation on top of the opening and no passivation. Since the bias is applied through the metallization, the strength of the electric field for the structure with no dielectric is the lowest in the middle of the optical opening (Fig. 4a green solid curve represents "no AlN" case). However, one can notice that with AlN deposited on top of the optical opening this effect is negligible (Fig. 4a, green dashed curve represents AlN-passivated case). Figure 4b shows the lateral electric field profile of the simulated CdTe sensor with the defect inclusion and passivation layer along the optical opening for different distances from the surface. The field is uniform across the sample except for a local fluctuation of the field ascribed to the defect inclusion. For the field 1 μm below the surface the distribution reaches a peak at 4560 V/cm, then for 5 μm the peak height is decreasing, at 10 μm there is still some disturbance of the field and after 40 μm it becomes uniform. Also the electric field strength is almost two times higher for the detector with a dielectric on top of the optical opening. In the simulation, a positive fixed oxide charge was used with the absolute value of Q_f equal to $1{\times}10^{12}$ cm^{-2}. With the AlN layer on top of the optical opening, the potential difference increases and the strength of the electric field changes to a higher value. In Fig. 5, a simulated transverse field distribution as well as corresponding transient currents are shown for different oxide charge values . It can be noticed that with the higher value of the interface oxide charge, the electric field strength has a higher value. For the corresponding current signals the higher value of the interface oxide charge gives a lower value of the amplitude of the signal.

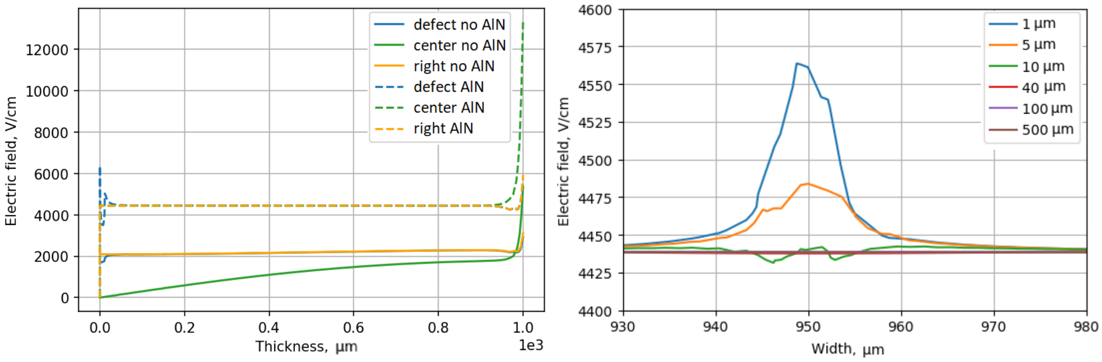

(a) (b)

Figure 4: a) Simulated transverse distribution of electrical field for the diode with the defect inclusion, no bulk traps and with and without passivation on top of the optical opening and b) lateral electric field cuts with AlN on top of the optical opening for different distances from the surface in μm in the proximity of the defect position.

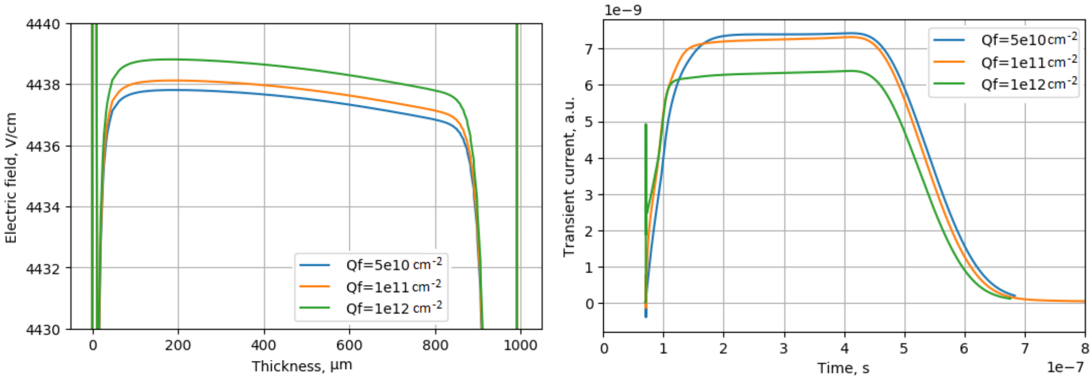

(a) (b)

Figure 5: a) Simulated transverse electric field distribution and b) corresponding transient current at the position of defect inclusion with AlN on top of the optical opening for different oxide charges Q_f.

The waveforms corresponding to electric fields with and without passivation in Fig. 4a are shown in Fig. 6. When there is no AlN film on top of the optical opening, the electric field is small enough that the signal duration is much longer than 1 μs. At the center of the opening without AlN film, the electric field near the surface is zero, so the charge carrier drift velocity slows in the low potential region and the signal evolves very slow. We see only the beginning of the signal with very low amplitude. On the right side of the opening, the current reproduces the signal with no defect in the Fig. 3a. The electric field strength at the center of the optical opening with the dielectric on top is almost the same as for the right side of the device, therefore the transient currents are identical as well. Comparing two transient signals at the position of the defect inclusion with and without passivation layer in Fig. 6, one can notice that the resulting current duration is 600 ns with the AlN deposited, while for the case without dielectric on the optical opening, the signal is longer than

1000 ns. The narrow peak in the beginning of the signal disappears with the passivation with the positive fixed charge, as the electric field strength increases, the electron drift velocity increased as well and the electrons are collected by the contact right away. It should be pointed out, that the shape of the signal with the defect inclusion and AlN on top of the opening has a characteristic form at the defect position, which can be easily identified from the surroundings.

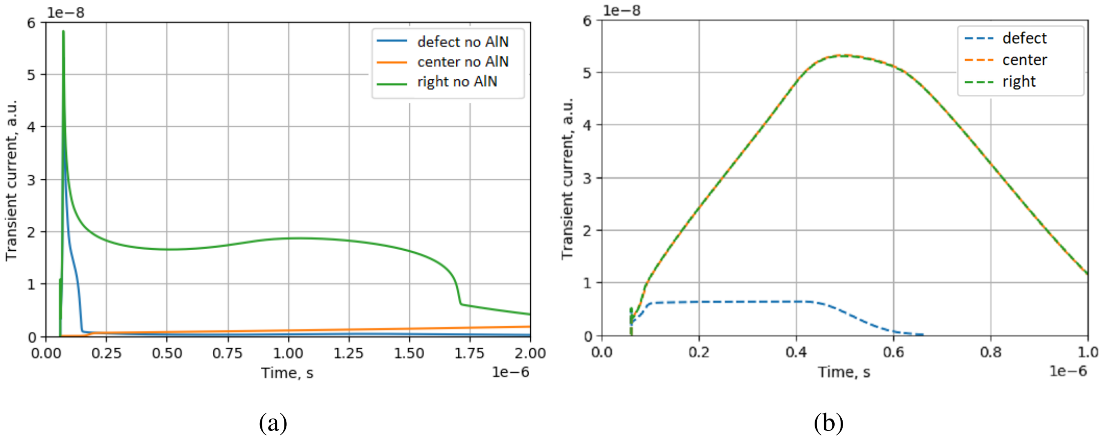

(a) (b)

Figure 6: a) Simulated transient current for simulated diode with the defect inclusion, no surface passivation and no bulk traps. b) Simulated transient current for simulated diode with the defect inclusion, surface passivation and no bulk traps.

Finally, the bulk trap levels were implemented as to take into account the highly defected CdTe bulk material. In order to reproduce the measured double peak electric field distribution, a new defect model was created. In the upper half of the structure, the acceptor trap level was introduced with the energy 0.72 eV from conduction band and electron and hole capture cross section $\sigma_{e,h} = 2 \times 10^{-13}$ cm^2. For the bottom half of the created diode, the donor level was implemented with the same energy level and electron and hole capture cross section of $\sigma_{e,h} = 1 \times 10^{-16}$ cm^2. The acceptor and donor concentration of 1×10^{12} cm^{-3} was used. The electric field distributions of the abovementioned structure are shown in Fig. 7a. In Fig. 7b the simulated transients are plotted. One can notice that the electric field shape reproduced by the waveforms and the transient signal amplitude at the position of the defect inclusion is around 4 times smaller than the signal at other positions of the device.

In a real CdTe crystal, there are different types of defect complexes that can be spread all over the bulk of the device [22], but in the simulation we used only one defect inclusion to see its effect on the waveforms. As an illustration of the dependence of the position and radius of the defect, Fig. 8a shows charge collection for different defect positions. The closer the defect inclusion is located to the diode surface, the higher is the impact of it on the red laser induced transient current. After around 19 μm from the surface there is no impact of the defect to the charge collection. In Fig. 8b the effect of the defect diameter is depicted. In this simulation, the defect inclusion is placed at 8 μm below the surface and the defect radius is varied. It is shown that for the smaller sized defect, a larger fraction of charge carriers reaches the diode backplane and thus the influence of the defect on the CCE is less. All the above transient current simulations were performed at the center position of the inclusion. However, if the laser beam was directed on the optical opening a

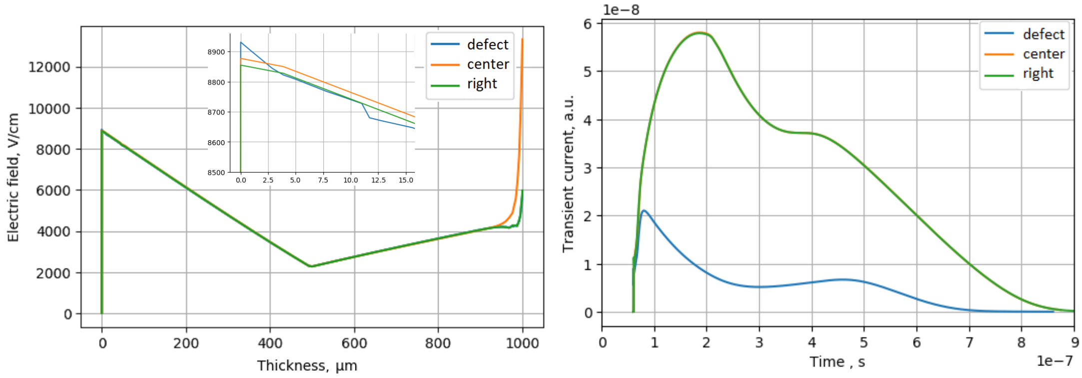

(a) (b)

Figure 7: a) Simulated transverse electric field distribution for the diode with the defect inclusion, bulk traps and passivation layer and b) corresponding transient currents.

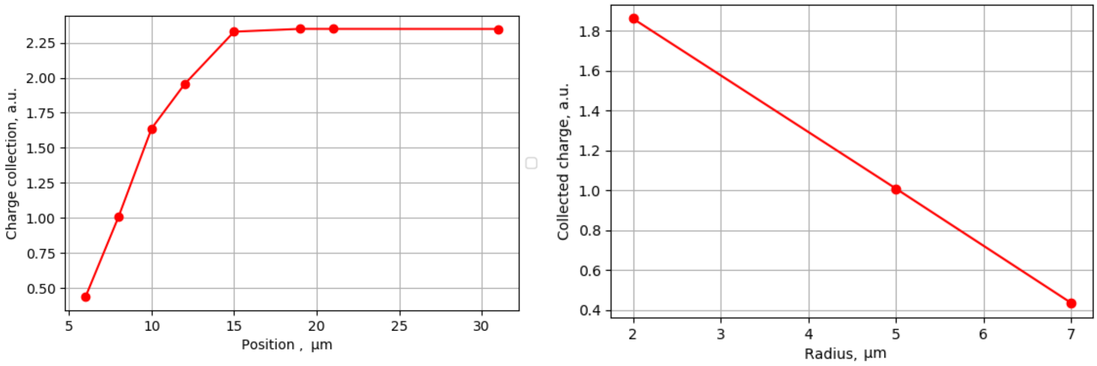

(a) (b)

Figure 8: Simulated charge collection for different a) defect positions with the radius 5 μm and b) different defect radius of the inclusion with the defect position of 8 μm below the surface. The beam diameter is 10 μm for both cases.

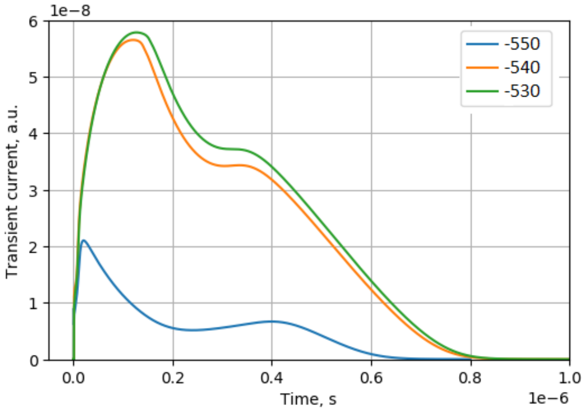

Figure 9: Simulated transient currents for the laser pointed at 3 different points at the optical opening where -550 is at the center of the defect.

bit shifted related to the defect center, the shape of the signal changes as well, as can been seen in Fig. 9. The closer the creation point of the charge carries is to the center of the defect, the more impact it has on the waveform.

3.2 Experimental results

By raster scanning the area of the opening in the horizontal direction, the uniformity of the detector is analyzed. The resulting plot of the CCE in the optical opening is presented in Fig. 10a. In the plot, the CCE is normalized to the maximum value in the area. The fact that there is a passivation layer deposited in our sample can be an explanation why there is no minimum of charge collection in CCE map. From Fig. 10b we can also see that in the low-CCE region, the drift velocity is also lower than on the upper half of the opening. This could be resulting from trapping and de-trapping of the carriers [23].

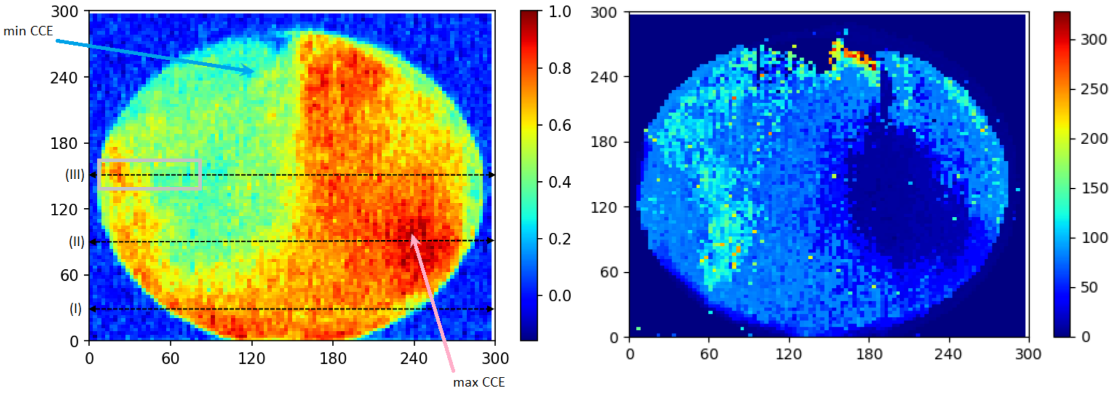

(a)

(b)

Figure 10: a) TCT area scan and b) the corresponding signal rise time at the optical opening of the CdTe detector at 660 nm. The area marked with a rectangle in (a) is discussed later in the paper.

The shape of the signals in the point with maximum and minimum CCE shown with the arrows in Fig. 10a and at the center of the optical opening are depicted in Fig. 11. The signal has a peak in the beginning and a long tail of the distributions that is produced both by the trapping-detrapping effects, and by the holes drifting to the sensor back-plane. The transient signal ends within 600 ns for the point with the lowest CCE, while the transient duration for the highest CCE is around 900 ns. The transient signal has a double peak shape [24]. Since the current is induced by charge moving in an electrical field, the shape of the signal is directly proportional to the electric field inside the sensor. The double peak signal gives us an evidence of the double peak electric field distribution through the bulk due to space charge build up at the contacts, probably in consequence of strongly trapped carriers in deep levels in the material [25].

In Fig. 12, the TCT signal cuts obtained from the oscilloscope at three different horizontal positions I, II and III of the TCT area scan map are depicted. These three horizontal cuts are shown in Fig. 10 with dashed lines and labeled. Each pixel represents a transient current amplitude where the x axis is a vertical position of the optical opening and y axis is a time of the waveforms. One can notice that from around 200 ns to 400 ns, the current signal has its minimum. For the TCT

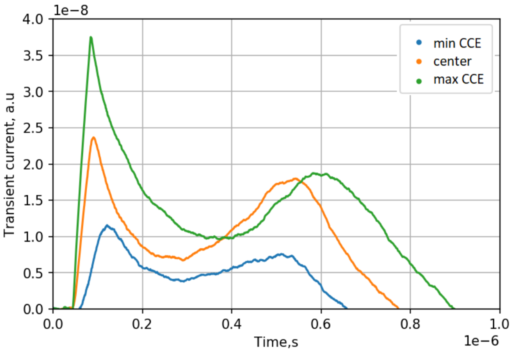

Figure 11: Transient currents for the point with maximum and minimum CEE shown with the arrows in Fig. 10a and at the centre of the optical opening .

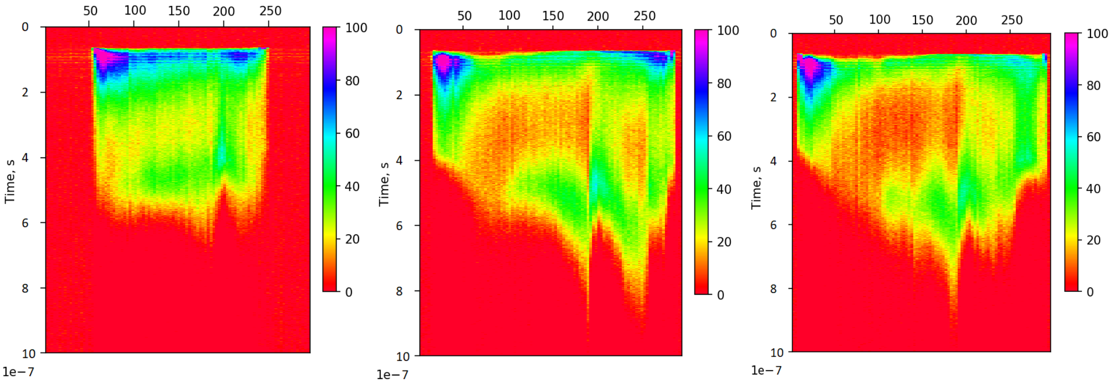

(a)

(b)

(c)

Figure 12: Transient current cuts at the I, II, and III horizontal position of the optical opening shown with dashed line in Fig. 10a.

signal cut at a horizontal position I, where we see a uniform distribution of charge collection in the CCE map, the waveform durations are almost equal comparing to the other cuts. Likewise there is a minimum of the signal height almost at the middle of the transient duration. For the cuts at the center of the optical opening line III and at the position II, the signal length is much more scattered and the minimum is more pronounced. The longer signal could be associated with a smaller value of electric field at this point. In contrary the shorter transient can indicate a higher field, or more likely a presence of some defect that can trap charge carries or act as charge drains, again leading to charge loss.

Figure 13a shows a closeup of the rectangular area marked in Fig. 10a. In Fig. 13b the measured transient currents at two points, with higher and lower CCE, from this area are depicted. The simulated signals are plotted with dashed lines. One can notice that the transient signal for the point B with the minimum CCE is well reproduced by the simulation with the defect inclusion. However, the simulated currents at the position A where the higher charge collection has occured, the simulation without any defect does not reproduce the measurement results precisely. This can be explained by the fact that in a real CdTe crystal, there are different types of defect complexes and they can be spread all over the bulk of the device. The simulation model with one defect works well in areas with a high concentration of defects, but may not be fully representative for such areas where defects are more sparse. Nonetheless, simulations demonstrate the ability of the transient current technique to be used in distinguishing between areas with high and low concentration of defects.

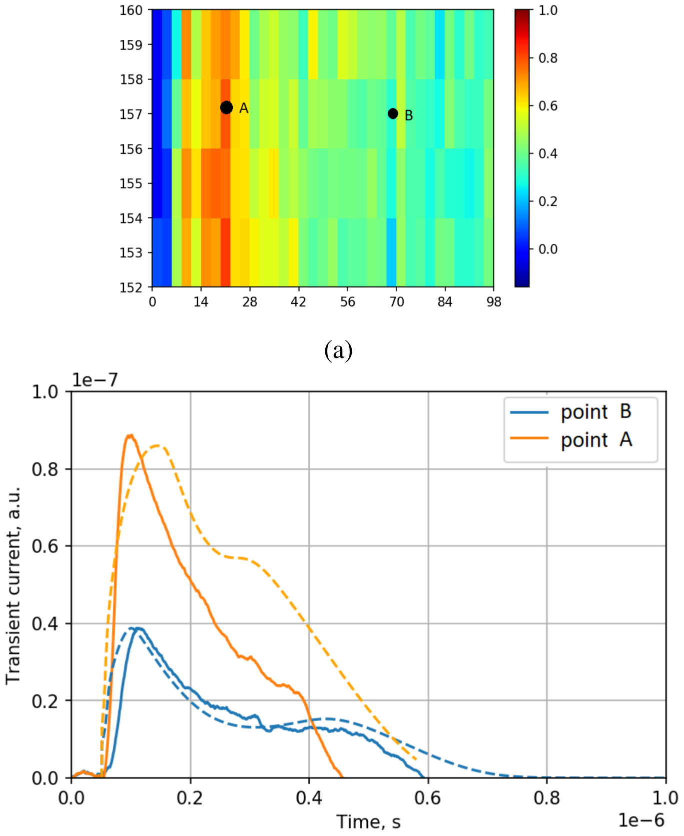

(a)

(b)

Figure 13: a) Zoomed part of the CCE map marked with rectangle in Fig. 10a. b) Simulated (dashed) and measured (solid) transient currents at the points A and B of the optical opening of the CdTe detector.

4 Conclusions

TCAD simulations are a powerful tool in aiding semiconductor detector design and understanding complex physical problems. Numerical simulations were used to create a model of a local bulk defect to better understand the effect of it on the transient current. This model shows that the presence of the local defect leads to a reduction in charge collection efficiency. Depending on the defect inclusion size, position and the position of the laser beam pointed on the surface of the optical opening, the transient current have different shapes. Defect inclusions that are closer to the surface and have a bigger diameter, if the trap level energies, trap concentration and electron and hole capture cross sections are unchanged, have a higher impact to the charge collection by red laser TCT. Shifted laser beam position from the center of the defect result in the fluctuations of the signal form as well. The surface passivation, especially the fixed oxide charge value, plays an important role in electric field formation and should be taken into account while designing the detector.

Simulation adds an evidence to the conclusion that the transient current has a characteristic shape at a defect position, which can be clearly distinguished from the surroundings using transient current technique. We were able to reproduce the measurement results adequately with a simple simulation model with one defect inclusion.

CdTe has a large amount of extended crystallographic defects that deteriorate the device performance. It is crucial to evaluate the quality of the material. A combination of the simulations, TCT and three-dimensional (3D) infrared microscopy (IRM) would show the impact of the localised defect of the raw material on the performance of the processed detector.

All measurements that were shown in this paper were made by using only one bias level, and at room temperature. Further studies will involve, among others, analysis of effects of bias level, impact of temperature variation, and changes in laser parameters.

Acknowledgements

The authors would like to thank Ruđer Bošković Institute for providing the facilities for CdTe measurements. S. Kirschenmann and S. Bharthuar thank Magnus Ehrnrooth foundation for financial support. Facilities for detector fabrication were provided by Micronova Nanofabrication Centre in Espoo, Finland within the OtaNano research infrastructure. The authors are grateful to Dr. Eija Tuominen and the Helsinki Detector Laboratory for providing the environment for electrical measurements. This study has been partially funded by the Horizon 2020 ERA Chair project, grant agreement 669014 (Particle and Radiation Detectors, Sensors and Electronics in Croatia, PaRaDeSEC). We acknowledge the funding by Academy of Finland project, number 314473, *Multispectral photon-counting for medical imaging and beam characterization*.

References

[1] H. Tsutsui, T. Ohtsuchi, K. Ohmori and S. Baba, *X-ray energy separation method using a CdTe semiconductor X-ray imaging sensor and photon counting method*, *IEEE Transactions on nuclear science* **40** (1993) 40–44.

[2] C. Szeles, *CdZnTe and CdTe materials for X-ray and gamma ray radiation detector applications*, *physica status solidi (b)* **241** (2004) 783–790.

[3] Y. Eisen, A. Shor and I. Mardor, *CdTe and CdZnTe X-ray and gamma-ray detectors for imaging systems*, *IEEE Transactions on Nuclear Science* **51** (2004) 1191–1198.

[4] A. Winkler, *Novel Detector Technologies for Medical Applications at the Example of Tumor Detection in BNCT*. PhD thesis, University of Helsinki, Finland, Oct., 2017.

[5] A. Winkler, T. Naaranoja, A. Gädda, J. Ott, P. Luukka, A. Karadzhinova-Ferrer et al., *Optical and electrical characterization of cadmium telluride x-ray pad detectors*, *Nuclear Instruments and Methods in Physics Research. Section A: Accelerators, Spectrometers, Detectors, and Associated Equipment* **924** (apr, 2019) 28–32.

[6] I. Visoly-Fisher, S. R. Cohen and D. Cahen, *Direct evidence for grain-boundary depletion in polycrystalline CdTe from nanoscale-resolved measurements*, *Applied physics letters* **82** (2003) 556–558.

[7] V. Eremin, N. Strokan, E. Verbitskaya and Z. Li, *Development of transient current and charge techniques for the measurement of effective net concentration of ionized charges (neff) in the space charge region of p-n junction detectors*, *Nuclear Instruments and Methods in Physics Research Section A: Accelerators, Spectrometers, Detectors and Associated Equipment* **372** (1996) 388–398.

[8] B. Dezillie, V. Eremin, Z. Li and E. Verbitskaya, *Polarization of silicon detectors by minimum ionizing particles*, *Nuclear Instruments and Methods in Physics Research Section A: Accelerators, Spectrometers, Detectors and Associated Equipment* **452** (2000) 440–453.

[9] G. Kramberger, *Advanced transient current technique systems*, Proc. Sci. **227** (2014) 032.

[10] Synopsys, "Synopsys webpage." https://www.synopsys.com, accessed on January, 2018.

[11] C.-H. Su, *Energy band gap, intrinsic carrier concentration, and fermi level of CdTe bulk crystal between 304 and 1067k*, *Journal of Applied Physics* **103** (2008) 084903, [`https://doi.org/10.1063/1.2899087`].

[12] A. Castaldini, A. Cavallini, B. Fraboni, P. Fernandez and J. Piqueras, *Deep energy levels in CdTe and CdZnTe*, *Journal of Applied Physics* **83** (1998) 2121–2126, [`https://doi.org/10.1063/1.366946`].

[13] A. Wardak, M. Witkowska-Baran, M. Szot, D. Kochanowska, B. S. Witkowski, A. Avdonin et al., *Electric field distribution around cadmium and tellurium inclusions within CdTe-based compounds*, *Journal of Crystal Growth* **533** (2020) 125486.

[14] H. Shiraki, M. Funaki, Y. Ando, S. Kominami, K. Amemiya and R. Ohno, *Improvement of the productivity in the growth of cdte single crystal by thm for the new pet system*, in *2007 IEEE Nuclear Science Symposium Conference Record*, vol. 3, pp. 1783–1787, 2007. DOI.

[15] A. Gädda et al., *Cadmium Telluride X-ray pad detectors with different passivation dielectrics*, Nucl. Instrum. Meth. A **924** (2019) 33–37.

[16] R. Van Overstraeten and H. De Man, *Measurement of the ionization rates in diffused silicon p-n junctions*, *Solid-State Electronics* **13** (May, 1970) 583–608.

[17] S. Ramo, *Currents induced by electron motion*, *Proc. Ire.* **27** (1939) 584–585.

[18] A. Gädda, A. Winkler, J. Ott, J. Härkönen, A. Karadzhinova-Ferrer, P. Koponen et al., *Advanced processing of CdTe pixel radiation detectors*, *Journal of Instrumentation* **12** (dec, 2017) C12031–C12031.

[19] J. M. Khosrofian and B. A. Garetz, *Measurement of a gaussian laser beam diameter through the direct inversion of knife-edge data*, Appl. Opt. **22** (Nov, 1983) 3406–3410.

[20] M. Kalliokoski et al., *Characterization and identification defects in CdTe detectors using scanning laser transient current technique*, in Proc. 2020 IEEE NSS/MIC/RTSD, Nov, 2020.

[21] M. O. Reese, C. L. Perkins, J. M. Burst, S. Farrell, T. M. Barnes, S. W. Johnston et al., *Intrinsic surface passivation of CdTe*, *Journal of Applied Physics* **118** (2015) 155305, [`https://doi.org/10.1063/1.4933186`].

[22] A. E. Bolotnikov, N. M. Abdul-Jabbar, O. S. Babalola, G. S. Camarda, Y. Cui, A. M. Hossain et al., *Effects of Te Inclusions on the Performance of CdZnTe Radiation Detectors*, *IEEE Trans. Nucl. Sci.* **55** (2008) .

[23] K. Suzuki, S. Seto, T. Sawada and K. Imai, *Carrier transport properties of HPB CdZnTe and THM CdTe:Cl*, IEEE Trans. Nucl. Sci. **49** (June, 2002) 1287–1291.

[24] V. Eremin, E. Verbitskaya and Z. Li, *The origin of double peak electric field distribution in heavily irradiated silicon detectors*, *Nuclear Instruments and Methods in Physics Research Section A: Accelerators, Spectrometers, Detectors and Associated Equipment* **476** (2002) 556–564.

[25] A. Cola and I. Farella, *The polarization mechanism in cdte schottky detectors*, *Applied Physics Letters* **94** (2009) 102113, [`https://doi.org/10.1063/1.3099051`].